Polarimetric Signatures from Natural and Artificial Randomly Distributed Targets

M. Chandra, V. Ziegler, A. Hornbostel, E. Lüneburg, A. Schroth

German Aerospace Research Establishment (DLR)
Institute for Radio Frequency Technology
D-8031 Wessling/Obb. - Germany

ABSTRACT

In this paper, initially, the essential measurement method of the DLR weather radar is described. In the following, some polarimetric signatures from natural and artificial targets (polarimetric DLR weather radar and JPL SAR measurements) are considered. The interpretation of these polarimetric signatures will include: (a) qualitative and quantitative meteorological deductions, (b) the use of complex correlations for determining three parameter rain drop size distributions, (c) estimation of attenuation along a satellite beacon, (d) the polarization dependence of radiometric sky noise temperature in the presence of precipitation, and (e) the use of the covariance matrix for analysing the polarimetric properties of different targets.

INTRODUCTION

Since the inception of the DLR radar, the measurement of the radar echoes corresponding to the four elements of the target backscattering matrix (henceforth S-matrix) in a user chosen orthogonal polarization basis has become possible.

Each of this four-fold data stream is recorded by linear coherent receivers as well as logarithmic power receivers. Such fully polarimetric radar measurements lend themselves to a vast variety of methods of data analysis in addition to the ones established in conventional polarimetric radar meteorology. To name a few: average correlations between various echoes, Doppler-moments, optimal-polarizations via the individual S-matrix measurements, the Mueller-matrix characterization, the coherency-matrix description and the covariance-matrix approach. The polarimetric DLR radar is therefore a versatile but complex system. A detailed description of the radar may be found in (Schroth, Chandra, Meischner, 1989).

Nevertheless, as a prelude it would be instructive to briefly recall the basic S-matrix concept that is required for understanding the present configuration of the DLR-radar. As described in (Chandra, Jank, Meischner, Schroth, Clemens, Ritenberg, 1986), it mutually orthogonal polarization states, represented by unit vectors $\hat{x}$ and $\hat{y}$, constitute the polarisation basis for radar measurement, then the relationship between transmit and receive EM-waves at the radar can be described as:

$$\begin{bmatrix} E_x \\ E_y \end{bmatrix}_{receive} = \frac{K}{r^2} \begin{bmatrix} S_{xx} & S_{xy} \\ S_{yx} & S_{yy} \end{bmatrix} \begin{bmatrix} E_x \\ E_y \end{bmatrix}_{transmit} \quad (1)$$

In this equation the r^2-dependence arises due to the two-way path covered by the signal in the transmit and receive traverse. Also, this range dependence term is factored out of the S-matrix in keeping with the natural separation of pulse volumes from range in pulsed radar systems. The actual radar measurement of this S-matrix, in practice, is realized in the following manner: first a radar pulse of polarization state $\hat{x}^+ = \hat{e}_1^+$, as shown in Figure 1, in transmitted and the ensuing echo (of whatever polarization) is received simultaneously in the co- and cross-polar receive channels corresponding to the orthogonally polarized receive polarizations $\hat{x}^- = \hat{e}_1^-$ and $\hat{y}^- = \hat{e}_2^-$, respectively. The co- and cross-polar echoes so received are simultaneously processed by both log-power and coherent linear receivers. The linear receivers detect these co- and cross-polar echoes as complex quadrature voltages $V_{xx} = I_{xx} + j\,Q_{xx}$ and $V_{yx} = I_{yx} + j\,Q_{yx}$, which, in turn, are proportional to the complex target S-matrix elements S_{xx} and S_{yx}. These measurements lead to the determination of the first column of the S-matrix in eq. (1). The same echoes, in the logarithmic receivers are detected ad co- and cross-polar powers P_{xx} and P_{yx} that are, respectively, proportional to the target backscatter cross-sections σ_{xx} and σ_{yx}. This combined processing of the co- and cross-polar echoes by linear- and log-receivers occurs for all range-bings along the 'radar-ray'.

Following this measurement, and interval $\delta t = 1/\mathrm{PRF}$ later, where PRF denotes the pulse repetition frequency, this process is repeated, this time, however, the trans-

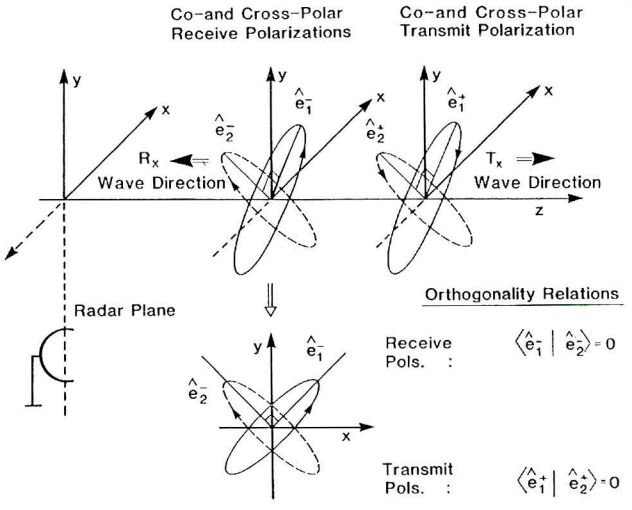

Fig. 1 - Mutually orthogonal polarization pairs of transmit and receive cases in relation to the radar-beam.

mitted radar pulse is of polarization state $\hat{y}^+ = \hat{e}_2^+$ and the receive co- and cross-polar channels correspond to receive polarizations $\hat{y}^- = \hat{e}_2^-$ and $\hat{x}^- = e_1^-$, respectively. Again these co- and cross-polar echoes are detected simultaneously by the linear and logarithmic receivers for all range-bins. The linear receivers, thus, deliver the complex quadrature voltages $V_{yy} = I_{yy} + j\,Q_{yy}$ and $V_{xy} = I_{xy} + j\,Q_{xy}$ which are proportional to the second column S-matrix elements S_{yy} and S_{xy}. The log-power receivers, on the other hand, deliver the corresponding co- and cross-polar powers P_{yy} and P_{xy} that are proportional to the target backscatter cross-sections σ_{yy} and σ_{xy}. In this measurements scheme, the elements in the two columns of the so measured S-matrix are temporally displaced by the time-interval δt. Therefore, in the polarimetric sense under the S-matrix concept, the DLR-radar registers a four-fold data stream arising from echoes proportional to the four elements of the quasi-instantaneous target S-matrix. Hence, the m-th radar measured S-matrix may be described as:

$$\begin{bmatrix} S_{xx}(t_m) & S_{xy}(t_m + \delta t) \\ S_{yx}(t_m) & S_{yy}(t_m + \delta t) \end{bmatrix}_{radar-measured} \qquad (2)$$

Typically the DLR-radar measures a total of M (known as the sample-size in radar parlance) such quasi-instantaneous S-matrices and the corresponding power-echo returns for all range-bins defined along a radar-ray. Due to buffer space and processing-time limitations, however, the DLR-radar in its present configuration is capable of saving as 'raw-data' only the full measurement series of the S-matrices (i.e. the linear receiver echoes) and the mean-values of power returns (averaged over sample-size) in the form of equivalent radar reflectivites for the four channels i.e. Z_{xx}, Z_{yx}, Z_{yy}, and Z_{xy}. This basic four-fold data-set collected by the DLR-radar in its present configuration is summarized in Figure 2. Furthermore, as detailed in (Schroth, Chandra, Meischner, 1989), a complex radar like the DLR-radar has for various different purposes (stemming from different observational requirements of radar measurables and scanning-pace, etc.) appropriately suited measurement modes, which among others include the Doppler-mode, the reflectivity mode (which contains Z_{DR} and LDR measurements), the S-matrix mode, and the time-series mode. Though these modes may vary in detail, their data-contents could, however, always be traced back to the basic four-fold data-set of radar echo measurements shown in Figure 2. Regarding the scanning options available with the DLR-radar, it, naturally, offers RHI, PPI and programmable slew scans. Additionally, it enables the user to automatically scan conical volume-shells by either a series of RHI- or PPI-cuts. Again, for further details the reader is directed to (Schroth, Chandra, Meischner, 1989).

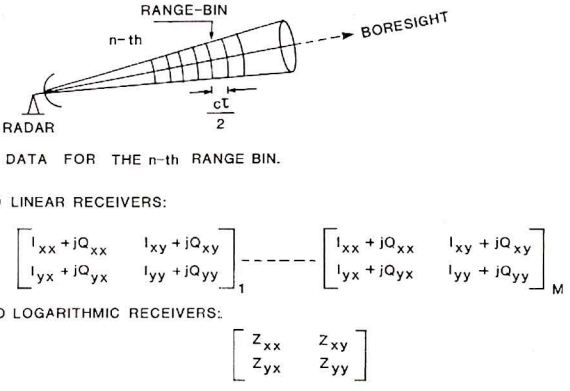

Fig. 2 - Summary of the basic data set currently available with DLR radar for a user chosen orthogonal polarization basis $\hat{x}$ and $\hat{y}$.

In order to orientate the reader toward the ensuing text, a brief description of the established polarimetric observables from radar meteorology will now follow. Naturally occuring precipitation such as rain, hail, ice-crystal clouds (e.g. cirrus clouds), etc., consists of particles (called hydrometeors) of oblate and/or prolate spheroidal shapes. In general, these particles fall under gravity with their rotational symmetry axis aligned either parallel or perpendicular to the gravitation vector. The degree of alignment, however, is a function of turbulence, electrostatic effects and wind shears. The latter can also induce canting. Such a collection of spheroidal particles bearing an overall degree of alignment, therefore, creates scattering anisotropy in precipitation volumes. This causes S_{hh} and S_{vv} echoes to differ in magnitude and in phase. In established radar meteorology the horizontal-vertical and left-right circular polarisation basis have found wide application.

In this connection, two radar observables have been extensively used: one, the differential reflectivity, Z_{DR}, and linear depolarization ratio, LDR, the other. They are defined as

$$Z_{DR} = 10 \log \frac{Z_{hh}}{Z_{vv}} \tag{3}$$

and

$$LDR = 10 \log \frac{Z_{hv}}{Z_{vv}} \; . \tag{4}$$

Here, typically, Z_{hh} and Z_{vv} represent horizontally and vertically polarized reflectivity factors respectively. It may also be noted that reflectivity, commonly measured in dBZ (dimension of Z is $mm^6 m^{-3}$), is proportional to the average backscattered echo power and thus to the total target backscatter cross-section. The average backscattered power may either be obtained from linear receiver measurements, i.e., $< | S_{hh} |^2 >$ or from log-power receiver measurements. With the DLR radar both methods are simultaneously available. Indeed, reflectivity can be seen as a special case of the generalized complex correlations described later in section 3.

The differential reflectivity Z_{DR} serves as an indicator of overall hydrometeor shape departure from the spherical form. In rain, this quantity can be shown to be related to the median volume drop diameter. The linear depolarisation ratio LDR is, on the other hand, proportional to the cross-polar signal strenght. It is thus an indicator of canting effects and turbulence.

1. POLARIMETRIC SIGNATURES OBTAINED WITH THE DLR RADAR AND THEIR ASSESSMENT

As demonstrative examples of polarimetric data, shown in Figure 3 to Figure 6 are the measurements of reflectivity factor, Z_{hh}, the differential reflectivity, Z_{DR}, the linear depolarization ratio, LDR, and the correlation factor for an RHI data-scan in rain due to the DLR-radar. Figure 3 reveals local areas of high reflectivity values > 35 dBZ situated below the height of 1.5 km. A melting band, not obvious in the reflectivity signature is, however, well established (in the form of enhanced values) at the height of 1 km in the differential reflectivity signature in Figure 4. The pressence of this melting band is similarly noticeable as enhanced values in the corresponding LDR signature of the event summarized in Figure 5. Both the LDR and the Z_{DR} signatures indicate that the melting band is close to the ground giving rise to rain mixed with wet snow in elevations close to the ground. Before considering the temporal correlation factor signature, we briefly define, in the current sense of usage, the term correlation factor as a percentage, i.e. (Chandra, 1991):

$$\left| \frac{< S_{hh}^{*}(t)\, S_{hh}(t + \Delta t) >}{< S_{hh}^{*}(t)\, S_{hh}(t) >} \right| \cdot 100 \; . \tag{5}$$

The correlation factor displayed in Figure 6 incorporates the correlation delay, (Chandra, 1991), of $\Delta t = 2/PRF$, where the pulse repetition frequency is in the present case 1200 Hz. The correlation factor, in general, is inversely related to the Doppler spectral width of the radar echoes but directly proportional to the radar echo decorrelation time. Physically, this quantity will reflect the temporal variation of the backscattering properties of the pulse volume influenced by the turbulence effects prevailing in the meteorological target. According to the consensus of opinion based on empirical observation of radar data, the correlation factor in rain is in the region of 95-100%. Values less than about 95% indicate the simultaneous presence of mixed-phase or ice-phase hydrometeors. Values as low as 50% have been reported in (Hendry, Cormick, 1974) and observed by the authors in presumably a hail-shaft radar volume. Details of the basic methodology of microphysical interpretation of quantities relating to complex correlations due to polarimetric radar echoes may be found in (Chandra, Schroth, Lueneburg, 1987), (Chandra, 1991) and (Chandra, Schroth, Lueneburg 1985).

Returning to the correlation data in Figure 6, values in the range of about 85-95% are observed around and below the height of 1 km. As stated earlier these values are less than the typical values observed in most pure rain cases. The physical explanation for this may be found in the fact that melting hydrometeors freely falling under gravity are associated with random lateral motions, (Mitra, Vohol, Pruppacher, 1988), therefore, one may expect to find in regions of mixed phase hydrometeors, as mentioned earlier, a higher degree of turbulence, which in turn would lead to smaller observed values of the correlation factor (i.e. due to reduced signal decorrelation times). This feature, once again, corroborates the mixed phase nature of the precipitation reaching the ground as observed in the signature in Figure 3 to Figure 5. In particular these considerations may also help to explain the origin of the LDR melting band seen in Figure 5: i.e. the turbulence in the melting band will cause the degree of overall hydrometeor alignment to decrease and thus the cross-polar return to increase.

In the foregoing discussion it has been demonstrated how polarimetric signatures could help in the identification of hydrometors. Applications of such methods should not only find use in pure atmosheric physics but also in critical weather observation around airports and motorways.

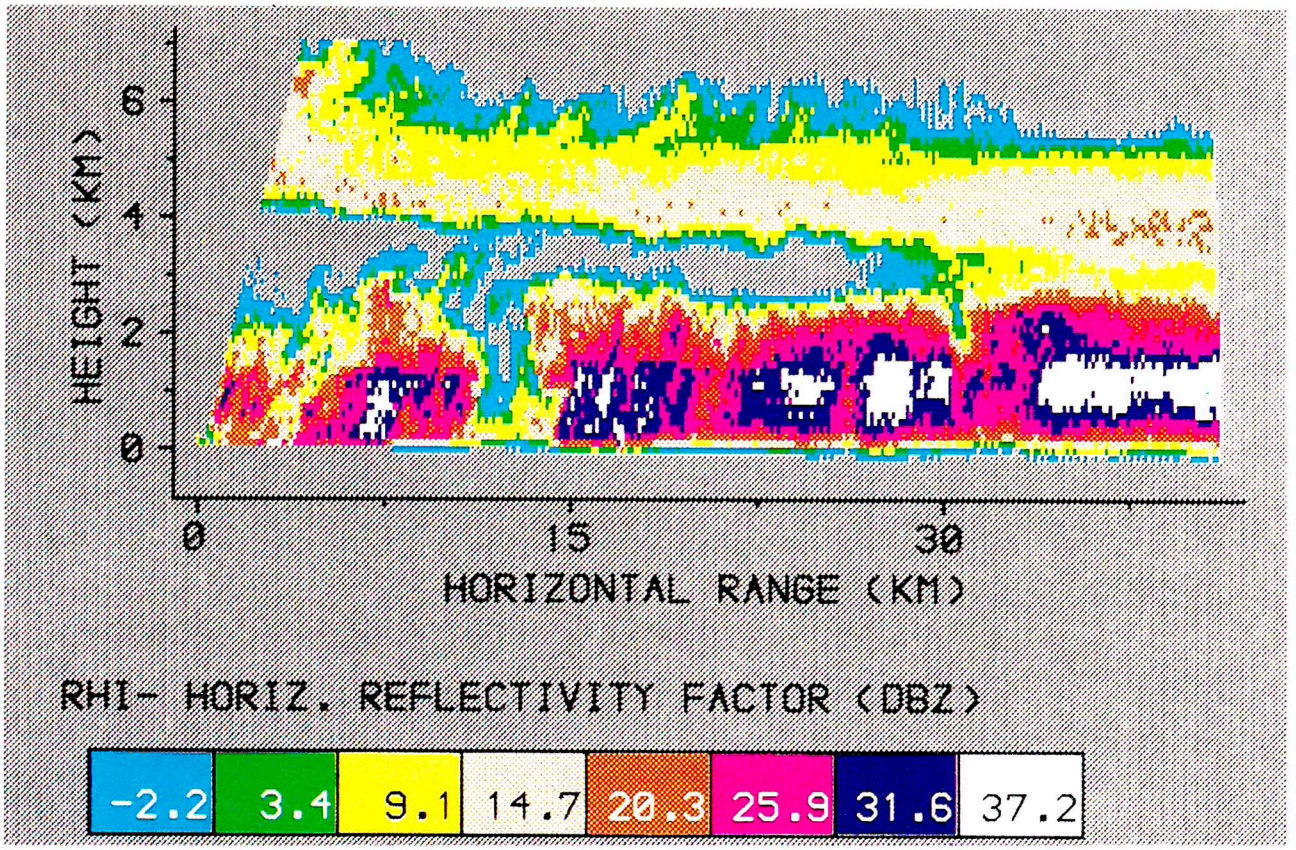

Fig. 3 - The reflectivity factor, Z_{hh}, signature due to an RHI-scan made by the DRL-radar on the 24-th of Sept. 1990. The DB value represents 10 log Z_{hh}.

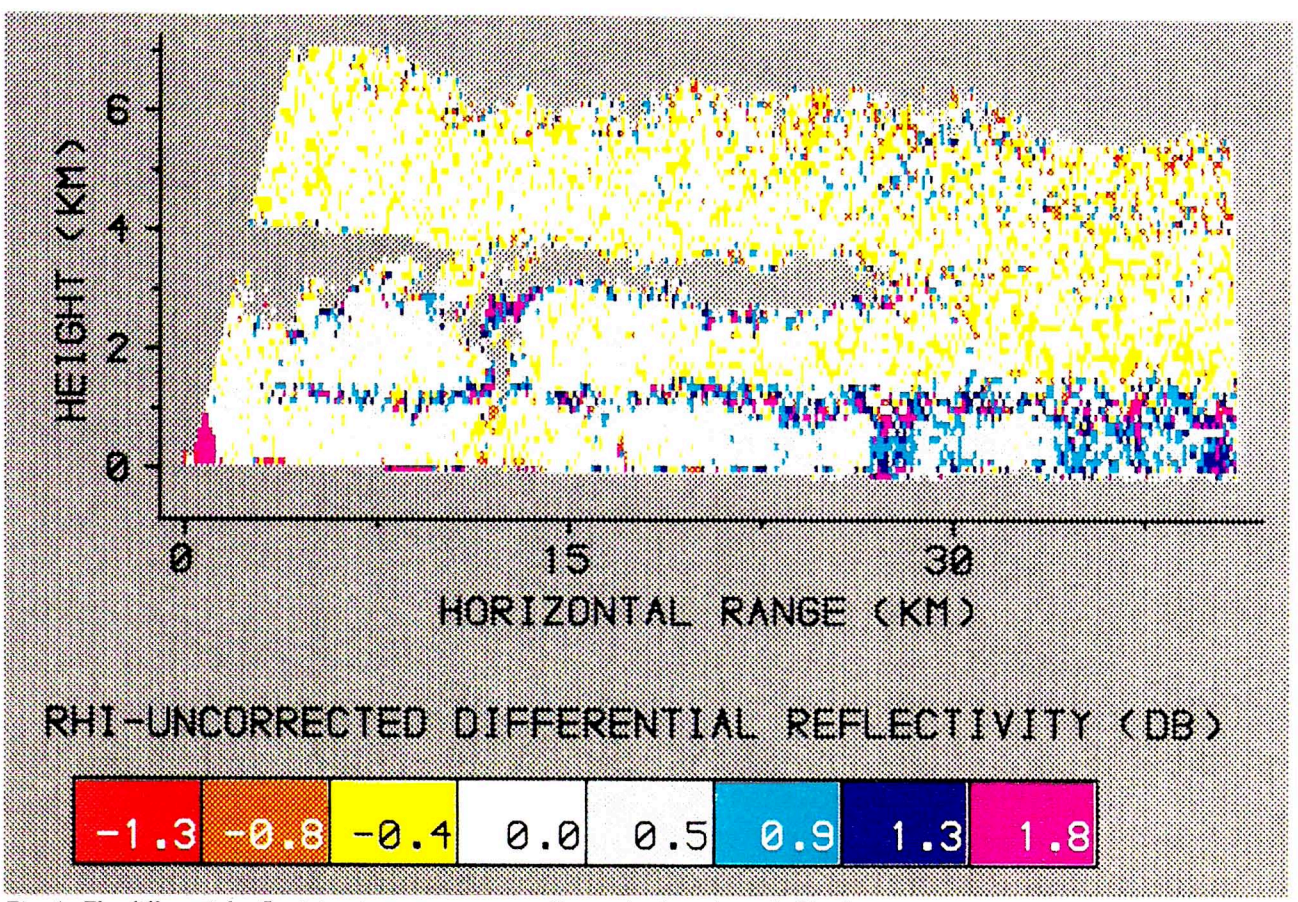

Fig. 4 - The differential reflectivity signature corresponding to the data shown in Fig. 3.

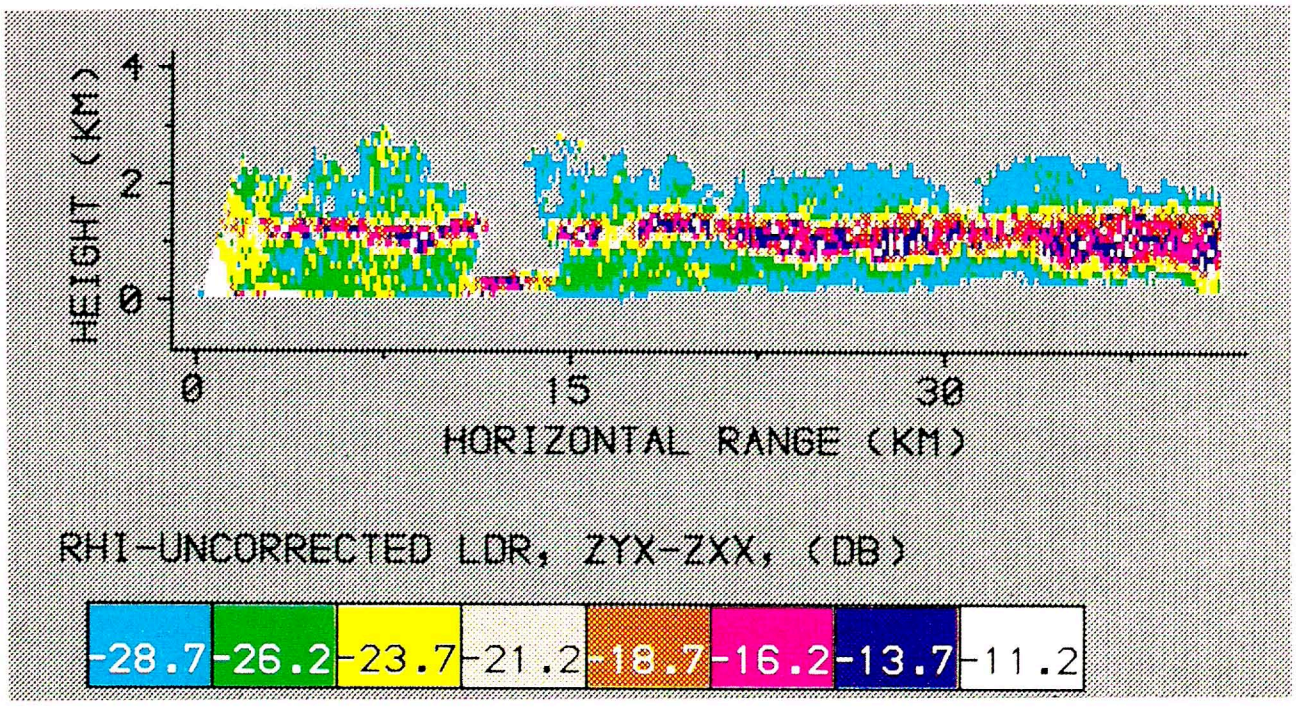

Fig. 5 - The linear depolarization ratio signature corresponding to the data shown in Fig. 3.

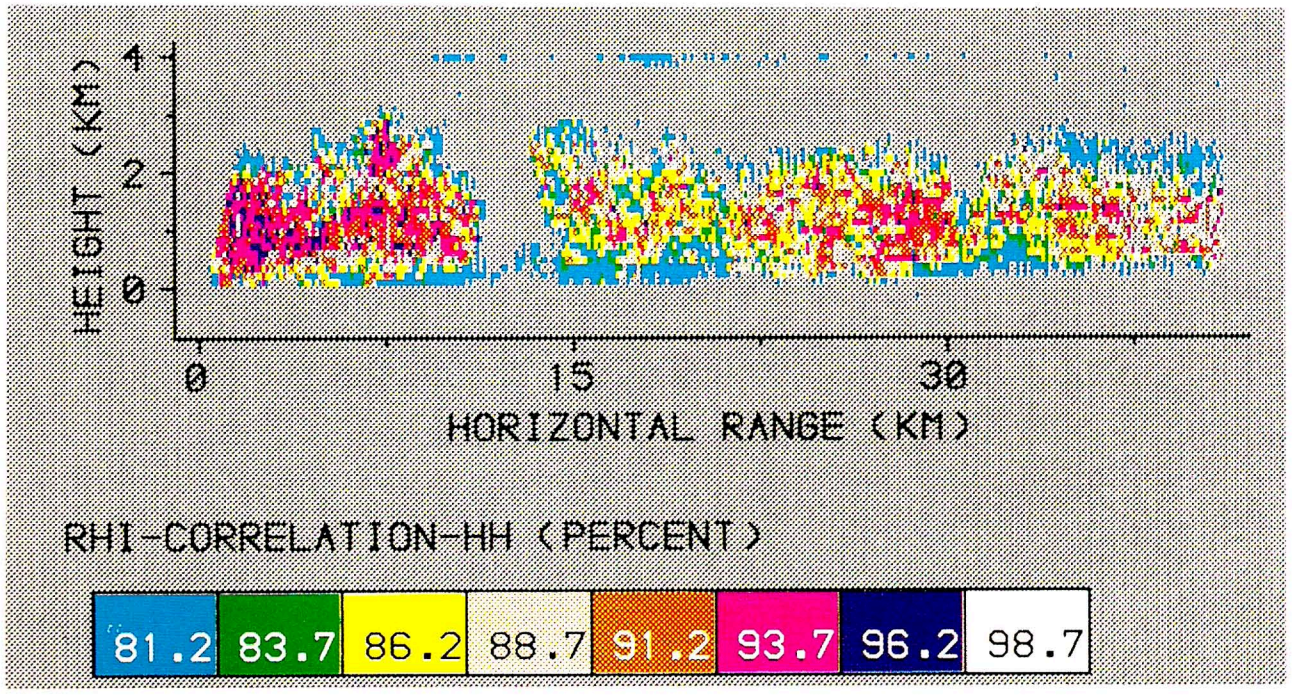

Fig. 6 - The signature of the correlation factor (defined in the text) corresponding to the data shown in Fig. 3.

2. DETAILED MICROPHYSICAL INTERPRETATION VIA POLARIZATION DEPENDENT COMPLEX CORRELATIONS BETWEEN POLARIZED RADAR ECHOES WITH THE DLR RADAR AND THEIR ASSESSMENT

The accuracy of the determination of rain intensity and rain induced microwave attenuation by radar depends crucially on the capability to estimate the raindropsize distribution from the measurements. From the conventional polarimetric methods, using Z_{DR} and Z_{hh} measurements, only two parameters (i.e. D_0 and N_0) of the following three-parameter raindropsize distribution could be determined:

$$N(D_e) = N_0 D_e^{\mu} \exp\left[-\frac{(3.67 + \mu) D_e)}{D_0} \right] . \quad (6)$$

Thus in the conventional polarimetric method the μ parameter remains undetermined. The significance of the μ parameters is indispensable when high temporal and spatial resolution for rain rate and propagation predictions are required. This situation can, however, be bettered by using the additional radar measurand:

$$arg\left[< S_{vv}^{*}(t)\, S_{hh}(t + \delta t) > \right] = arg\left[\chi_{hh}^{vv}\left(R_N , (\delta t)_{hh} \right) \right] \quad (7)$$

The microphysical interpretation of this quantity, $\chi_{hh}^{vv}\left(R_N , (\delta t)_{hh} \right)$, as shown in (Chandra, Schroth, Lueneburg, 1987), (Chandra, 1991), and (Chandra, Schroth, Lueneburg, 1985) reveals with reference to Figure 7:

$$\chi_{hh}^{vv}\left(R_N , (\delta t)_{hh} \right) = C_{hh}^{vv} \exp\left[-j \left(K_{hh} - K_{vv}^{*} \right) R_N \right] x$$

$$x \int_0^{(D_e)_{max}} N(D_e) \overline{\left[S_{vv}^{*}(D_e , t)\, S_{hh}(D_e , t + (\delta t)_{hh}) \right]} \exp$$

$$\left[-j \left(k_{hh} \overline{v(D_e)} \right) (\delta t)_{hh} \right] dD_e \, x \quad (8)$$

$$x 2\pi \int_{r'=0}^{c\tau/2} \int_{\Theta=0}^{\Theta_v/2} \exp\left[-j \left(k_{hh} - k_{vv}^{*} r' \right) \right] W_1^2(r')\, W_2^2(\Theta) x$$

$$x (R + r')^2 \sin(\Theta)\, dr'\, d\Theta$$

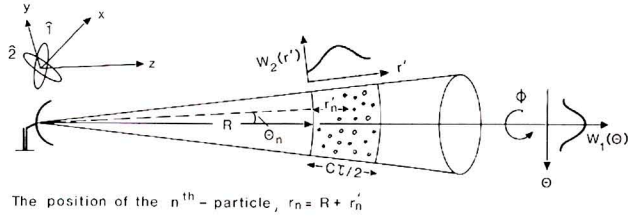

Fig. 7 - The basic underlying radar geometry. Note, R here is referred to as R_N in the text.

Here, C_{hh}^{vv} is a system and polarization dependent complex constant, $K_{hh} = K_h^{-} + K_h^{+}$ is the effective external two-way complex propagation constant accounting for the echo signal traverse between the radar and the near edge of the N-th scatter-volume. K_{vv} is similarly defined; $k_{hh} = k_h^{-} + k_h^{+}$ and $k_{vv} = k_v^{-} + k_v^{+}$ are the corresponding internal (i.e. within the N-th pulse volume) effective propagation constants. k_{hh} is related to the internal propagation constant of the temporally trailing echo and is thus also the one appropriate for registering Doppler-induced effects. $\overline{v(D_e)}$ is the mean radial velocity of the hydrometeor of size D_e;

$\overline{S_{vv}^{*}(D_e , t)\, S_{hh}(D_e , t + (\delta t)_{hh})}$ is the mean product of the appropriate scattering amplitudes. $W_1(r')$ is the one-way receiver bandwidth related amplitude weighting function; $W_2(\Theta)$ is the two-way antenna pattern related (assuming rotational symmetry about the beam) amplitude weighting function. Again a detailed derivation of the equation above, its microphysical interpretation, and its applications, which are to be soon formally published, may nevertheless, currently be found in the conference papers (Chandra, Schroth, Lueneburg, 1987), (Chandra, 1991) and (Chandra, Schroth, Lueneburg, 1985).

Also shown in these sources is that the accumulative differential propagation phase accrued in the region bounded between the N-th and the (N + M)-th radar range bin could be retrieved from $\chi_{hh}^{vv}(R_N , (\delta t)_{hh})$ and $\chi_{hh}^{vv}(R_{N+M} , (\delta t)_{hh})$, providing these quantities are corrected for Doppler phases. Shown in Figure 8 is one such sample calculation. The various curves shown in the figure are typically physical quantity versus range. These quantities are (starting with the lowest curve): the horizontally polarized reflectivity factor, the corresponding differential relectivity, the Doppler-corrected phase argument of $\chi_{hh}^{vv}(R_N , (\delta t)_{hh})$ with the best linear fit through the data used for obtaining the best value of 2.8 degrees for the propagation phase that shows as the increment along the vertical axis.

The topmost curve shows the dependence of the corresponding propagation phase values obtained for different μ values using the N_0 and D_0 parameters derived from the physical model that use the reflectivity and the differential reflectivity measurements. A comparison of the measured accumulative differential propagation phase (2.8 degrees) against the two-parameter-model values reveals the best agreement for a μ value of about 9. This fact enables the calculation of rain rate along the radar ray using all three parameters of the rain drop size distribution.

Usually, when the μ parameter is not known a value of 0 is assumed. The second curve from the top in Figure 8 displays the difference in the radar rain rate predictions using the 'default' value and the 'radar determined effec-

tive' value of the μ parameters. The default value (i.e. the two parameter method) reveals an overestimate which has been frequently reported with the conventional rainrate estimation method. This specific example shows the potential of polarimetric methods in the field of quantitative radar meteorology. Indeed a full account of the forgoing discussion and theory is expected to be formally published in the near future.

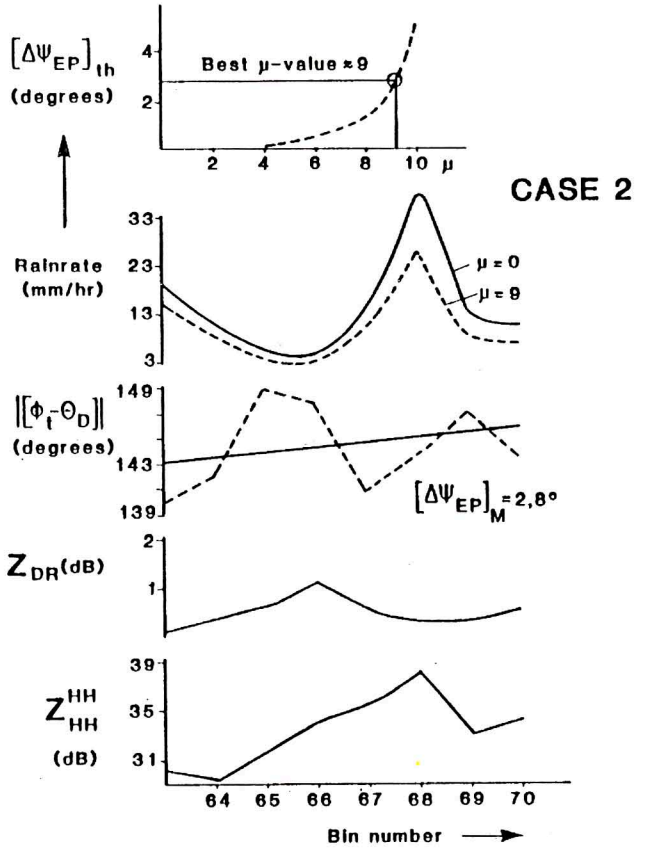

Fig. 8 - This illustration shows the stages for the radar determination of the μ parameter. The lower three profiles show the Z_{hh}, Z_{DR} and the Doppler corrected arg $[\chi^{vv}_{hh}(R_N, \delta t)]$ dependence in range (as bin numbers). From the third profile the accumulated differential propagation phase $[\Delta\Psi_{EP}]_M = 2.8^0$ is detailed. Comparison (shown in the topmost curve) against the corresponding calculated values (using XZ_{hh} and Z_{DR} information with different choices of μ values) yields the effective μ value over the range path considered. The rainrate profiles for μ = 0 and the radar determined value μ = 9 reveal an overestimate with former choice.

3. COMPARISON OF RADAR PREDICTED ATTENUATION ON AN EART-SATELLITE-PATH WITH OLYMPUS BEACON AND RADIOMETER MEASUREMENTS

In order to gain long time attenuation statistics the quasi horizontally polarized Olympus beacon signal at 19.77 GHz has been measured together with the radiometric sky temperature at 19 GHz along the same polarization continuously since September 1990. The equipment of the ground station includes also an optical distrometer and several meteorological instruments to measure the ambient temperature, the humidity, the pressure, the speed and the direction of the wind and the rain rate.

Accompanying measurements with the DLR coherent C-band weather radar, located at a distance of 350 m from the beacon receiving station, have been carried out. These measurements include both scans, which sample exactly along the Eart-satellite path by computer control, as well as RHI measurements in the azimuth direction to the Olympus satellite, allowing a parallel slant path to be extracted. From the measured polarimetric radar backscattering observables microphysical model parameters of rain, snow and ice clouds are derived and utilized to predict the line-of-sight propagation properties, in particular the copolar attenuation, differential attenuation, *XPD*, and differential phase on the Eart-satellite path at the beacon frequency (Schnablel, 1988).

The scattering amplitudes of non spherical rain drops have been calculated with the point matching method for both the radar frequency of 5.5 GHz and the beacon frequency. With the aid of these coefficients the two unknown parameters N_0 and D_0 of a two parameter exponential rain dropsize distribution

$$N(D_e) = N_0 \exp^{-3.67 D_e/D_0} \tag{9}$$

are computed from the measured values of the effective radar reflectivity factor along horizontal polarization, Z_{hh}, and the differential reflectivity $Z_{DR} = Z_{hh}/Z_{vv}$ for each range bin. The two parameter dropsize distribution is used because the determination of the third parameter μ (see eq. (6)) is not possible in an operational manner with the current DLR weather radar configuration. From these microphysical parameters the transmission matrices at both frequencies can be determined. The transmission matrices at 5.5 GHz are used to correct successively the measured reflectivities for propagation effects at the radar frequency. The transmission matrices at 19.77 GHz have to be transformed first to the adequate polarization plane of the beacon signal, which is received with a tilt angle of 24.3 degrees and an elevation of 27.6 degrees. Finally, the propagation parameters of the slant path at the beacon frequency are calculated by multiplication of all transmission matrices pertaining to the path.

Figure 9 shows the 10 s mean values of the copolar attenuation derived from the received beacon level and calculated from the sky temperature (ref. to eq. (10)) of a selected stratiform rain event. The radiometer attenuation is shifted for + 1 dB, so that it can be better distinguished from the beacon attenuation. Both are very highly correlated. The radar predicted copolar quasi horizontal at-

tenuation with regard to the tilt angle of the Olympus beacon signal is included in this figure.
Here slew scans had been applied. The required time for one scan was approximately 1 minute in this case. This sampling rate is too low to give a sufficient time resolution of the attenuation structure, see time span around 10.92, but in general also the radar prediction shows a good correlation with the measured attenuation of the beacon.
The radar prediction includes only the attenuation due to rain. For the comparison with the beacon attenuation the melting and the atmospheric attenuation due to water vapour and oxygen are added in Figure 9. The average melting band contribution (0.7 dB) was calculated from the reflectivities just below the bright band (Dissanayake, McEwan, 1978), (COST project 205) and the atmospheric contribution (0.5 dB) according to CCIR formulas (CCIR (Study Group V, 1986).

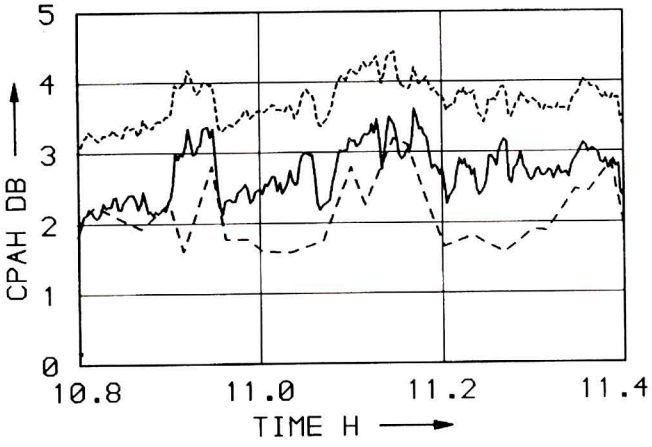

Fig. 9 - Copolar horizontal attenuation during stratiform rain on 31st Oct. 1990, (dotted) line: radiometer attenuation shifted for + 1dB, full line: beacon attenuation, dashed line: radar prediction).

4. POLARIMETRIC MEASUREMENTS OF THE SKY NOISE

The extinction of a microwave signal by a volume of hydrometeors is due to absorption and scattering. To include the multiple scattering effects, and effective medium temperature $T_m \approx 250 - 270K$, which is lower than the physical medium temperature, is introduced in the radiometric formula.

$$T'_{sky} = T_m (1 - \exp^{-c\,l}) \qquad (10)$$

where c is the extinction coefficient and l the path lenght. T_m depends on the extinction itself and was computed with the equation of radiative transfer for spherical drops and different rain cell models by some authors, e.g. Brussard (Brussard, 1984) and Asayesh (Asayesh, 1984).

The extinction and scattering cross sections of nonspherical rain drops have been calculated by Morrisson and Cross (Morrisson, Cross, 1974) for horizontal and vertical polarization at 18.1 GHz. They were related to the extinction coefficients of different rain rates by integrating over the two parameter dropsize distribution (eq. (9)). With these inputs the effective medium temperature T_m and the sky temperatures $T_{sky,h}$ and $T_{sky,v}$ along both polarizations were computed for a homogeneous atmosphere (vertical slab of 4 km, elevation: 0°). The results are given in Figure 10. Here N_0 was varied between 80 and $8 \cdot 10^7 mm^{-1} m^{-3}$ and D_0 was computed for rain rates between 1 and 30 mm/h by inversion of the following equatin (Atlas, Ullbrich, 1977).

$$R = 33.3 \int_0^\infty D^{3.67} N(D)\, dD$$

$$(R \text{ in } mm/h\,,\ D \text{ in } cm\,,\ N \text{ in } cm^{-1} m^{-3}) \ . \qquad (11)$$

The results are given in Figure 10. The full line represents the Marshall-Palmer dropsize distribution. The behaviour of $T_{sky,h}$ and $T_{sky,v}$ versus the rain rate is shown in (Hornbostel, Schroth, Preissner, 1991). The absolute sky temperature $T_{sky,h}$ increases with the rain rate. Also the differential sky temperature $T_{sky,h} - T_{sky,v}$ first increases, but then decreases again at the higher rain rates due to the saturation effect, i.e. the absolute sky temperature in both polarizations approaches an upper limit, which cannot be heigher than the physical rain temperature. The calculations shown in this figure are only applicable to rain rates less than 30 mm/h, because they do not take into account the depolarization by the medium. At higher rain rates the vector form of the equation of radiative transfer should be applied (Chandrasekhar, 1960), (Ishimaru, Cheung, 1980).

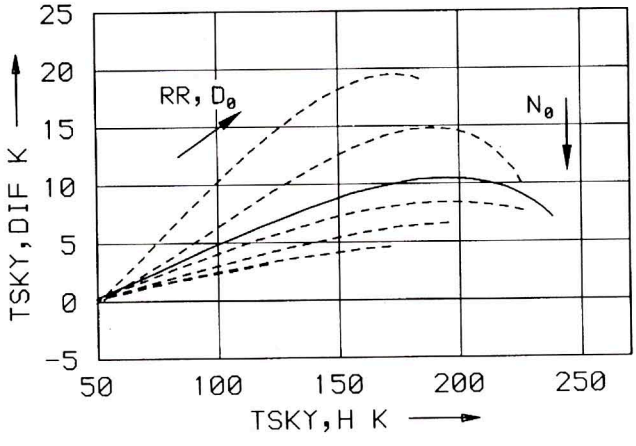

Fig. 10 - Calculated sky temperatures of a vertical slab (f = 18.1 GHz, d = 4 km, T_{amb} = 270K, clear sky attenuation: 0.8 dB, $N_0 = 80 \ldots 8 \cdot 10^7\ mm^{-1} m^{-3}$, rain rate: 1 ... 30 mm/h, full line: Marshall-Palmer drop size distribution).

Figure 11 shows the differential sky temperature between horizontal and vertical linear polarization measured by the polarimetric radiometer at 19.25 GHz with an elevation of 27.6° versus the absolute temperature $T_{sky,h}$. Another example of such a measurement is given in (Hornbostel, Schroth, Preissner, 1991) for a 20 minutes period. Similar to the radar Z_{DR} technique two parameter models, e.g. a two parameter dropsize distribution, may be derived from the differential sky temperature, if the general weather conditions are known from ground measurements. For the development of applicable algorithms of the rain cloud, which has a sizeable effect on the sky temperature ((Brussard, 1984) p. 34-36), may be obtained by accompanying radar measurements. Due to the fact that the radiometer measures the integral effects of the total path through the atmosphere, the parameters obtained from polarimetric radiometer data are only physically meaningful in this context in the case of a homogeneous atmosphere. Otherwise, they may be used as effective mean values for an equivalent homogeneous path.

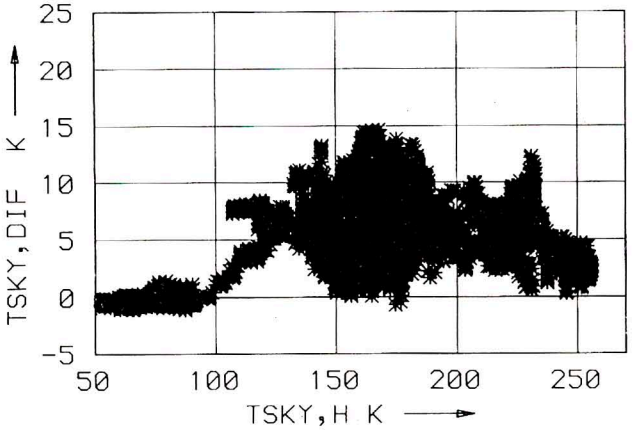

Fig. 11 - Differential sky temperature versus adsolute sky temperature $T_{sky,H}$ during four hours of stratiform rain on 25th Aug. 1990 (f = 19.25 GHz, elevation: 27.6°).

5. ANALYSIS OF RADAR RANDOM TARGETS VIA THE POLARIMETRIC COVARIANCE MATRIX

The polarimetric covariance matrix concept with its polarization invariant parameters can be used as a tool for polarimetric analysis.

Covariance matrix analysis for reciprocal random targets may be performed by unitary similarity transformations preserving important polarimetric invariances. An eigenvalue analysis provides important target related information.

The covariance matrix contains measurable radar observables and is directly linked to the statistics of the elements of the scattering matrix which determines the instantaneous backscattering features of a target.

A target feature vector in the arbitrary orthonormal {A,B} basis is introduced (Tragl, 1990)

$$\Omega\,(AB) = \left[\, S_{AA}\ \sqrt{2}\ \ S_{AB}\ S_{BB} \,\right]^T \tag{12}$$

The corresponding polarimetric covariance matrix is defined as

$$\Sigma\,(AB) : = < \Omega\,(AB)\ \Omega\,(AB)^+ >$$

$$= \begin{bmatrix} < |S_{AA}|^2 > & \sqrt{2} < S_{AA}\ S_{AB}^* > & < S_{AA}\ S_{BB}^* > \\ \sqrt{2}\ < S_{AB}\ S_{AA}^* > & 2 < |S_{AB}|^2 > & \sqrt{2} < S_{AB}\ S_{BB}^* > \\ < S_{BB}\ S_{AA}^* > & \sqrt{2} < S_{BB}\ S_{AB}^* > & < |S_{BB}|^2 > \end{bmatrix} \tag{13}$$

In eq. (13) $^+$ denotes the Hermitian adjoint and angular brackets indicate temporal (spatial) ensemble averaging assuming stationarity (homogeneity) of the random scattering medium.

In general, the positive semi-definite Hermitian matrix $\Sigma\,(AB)$ contains all second order moments of the target scattering coefficients. For a deterministic target, spatial or temporal ensemble averaging becomes obsolete and $\Sigma\,(AB)$ has rank 1.

The general polarimetric covariance matrix is derived from Σ_0 in the linear {HV} basis by means of a unitary similarity transformation.

$$\Sigma \equiv \Sigma\,(\rho) = < \Omega\,(\rho)\ \Omega^+\,(\rho) >$$

$$= T\,(\rho) < \Omega_0\ \Omega_0^+ > T^+\,(\rho) \tag{14}$$

$$= T\,(\rho)\ \Sigma_0\ T^+\,(\rho)$$

with the unitary unimodular 3 × 3 matrix

$$T\,(\rho) = \frac{1}{(1 + \rho\rho^*)} \begin{bmatrix} 1 & \sqrt{2}\ \rho & \rho^2 \\ -\sqrt{2}\ \rho^* & (1 - \rho\rho^*) & \sqrt{2}\ \rho \\ \rho^{*2} & -\sqrt{2}\ \rho^* & 1 \end{bmatrix} \tag{15}$$

where

$$T\,(\rho)\ T^+\,(\rho) = I \tag{16}$$

$$\det T\,(\rho) = 1\ . \tag{17}$$

Note that the norm of Ω is a target invariant with respect to the transformation of the following eq. (18)

$$\Omega\,(AB) = T\,(\rho)\ \Omega\,(HV) \tag{18}$$

The variable ρ is the so-called complex polarization ratio which completely determines the geometric parameters

φ (orientation angle) and τ (ellipticity) of the polarization ellipse according to

$$\rho = \frac{\cos(2\tau)\sin(2\varphi) + j\sin(2\tau)}{1 + \cos(2\tau)\cos(2\varphi)} \tag{19}$$

and conversely

$$\varphi = \frac{1}{2} arctan\left[\frac{2Re\{\rho\}}{1 - \rho\rho^*}\right] + \pi\, mod\,(\pi) \tag{20}$$

$$\tau = \frac{1}{2} arcsin\left[\frac{2Im\{\rho\}}{1 + \rho\rho^*}\right] \tag{21}$$

The covariance matrix Σ can now be expressed as a function of ρ

$$\Sigma(\rho) = \begin{bmatrix} P_{co}^A(\rho) & \sqrt{2}\,R_x^A(\rho) & R_{co}(\rho) \\ \sqrt{2}\,R_x^A(\rho)^* & 2P_x(\rho) & \sqrt{2}\,R_x^B(\rho)^* \\ R_{co}(\rho)^* & \sqrt{2}\,R_x^B(\rho) & P_{co}^B(\rho) \end{bmatrix} \tag{22}$$

Its main diagonal elements are mean backscattered copolar powers $P_{co}^A(\rho), P_{co}^B(\rho)$ and mean crosspolar power $P_x(\rho)$ as a function of the complex polarization ratio ρ . $R_x^A(\rho)$ and $R_x^B(\rho)$ will denote the correlation of backscattered orthogonal wave components if polarization A or B is transmitted. $R_{co}(\rho)$ signifies the correlation of the copolar scattering coefficients S_{AA} and S_{BB}.
Once the covariance matrix has been measured in one basis, e.g. Σ_0 in the {H, V} basis, it can easily be determined analytically for any other basis.

Familiar polarimetric signatures are obtained when plotting the mean power return and signal correlations as functions of the complex polarization ratio ρ or of the geometrical polarization parameters τ and φ (cf. eqs. (20) and (21)).
As an example, two different types of target areas as part of a synthetic aperture radar (SAR) image of the Oberpfaffenhofen test site will be considered. The data has been analysed at DLR Oberpfaffenhofen; Hel et al. (Held, Brown, Freeman, Klein, Zebker, Sato, Miller, Nguyen, Lou, 1988) give a description of the NASA-JPL airborne SAR-system.

The copolar and crosspolar power signatures for an area of grass in Figure 12 resembles a deterministic target, namely an ideally reflecting flat plate. Copolar power maxima are to be found for linear polarizations, whereas circular transmitter polarizations yield crosspolar maxima.
The covariance matrix of the considered area of buildings clearly indicates a random target (see eigenvalue spectrum). Looking at the power signatures in Figure 13, however, it turns out that the covariance matrix of this area may be approximately modelled by the sum of a corner reflector type (dihedral), and a noise covariance matrix. Similar signatures can be obtained for

- degree of coherence

$$\mu_{AB}(\rho) = \frac{|R_x^A(\rho)|}{\sqrt{P_{co}^A(\rho)\,P_x(\rho)}} \tag{23}$$

- degree of polarization

$$P_{AB}(\rho) = \frac{\left\{\left[P_{co}^A(\rho) - P_x(\rho)\right]^2 + 4\,|R_x^A(\rho)|^2\right\}^{1/2}}{P_{co}^A(\rho) + P_x(\rho)} \tag{24}$$

as function of ρ (Born, Wolf, 1964), (Tragl, 1990).
In the following table target invariant parameters of the covariance matrices of a representative area of buildings and an area of grass are given.
It should be remembered that a deterministic target has eigenvalues $\lambda_1 = \lambda_2 = 0$.

Table 1. Invariant parameters of two different target areas within an L-Band SAR-image of the Oberpfaffenhofen test site; the eigenvalues λ of the target covariance matrices have been normalised by the trace of the matrices.

Area	λ_1	λ_2	λ_3	$\Delta\lambda$	trace (Σ)
Grass	0.06	0.14	0.79	0.73	35.7 dB
Building	0.01	0.27	0.72	0.71	23.5 dB

The target invariant eigenvalues of the covariance matrix λ_i (i = 1,2,3) comprise interesting information on random target polarimetric backscattering features.

- The smallest eigenvalues λ_1 and λ_2 indicate the degree of randomness of the target. For a deterministic target $\Sigma_0 = \Omega_0\,\Omega_0^+$ and invoking the spectral theorem of matrix algebra (Lancaster, Tismenetsky, 1985) one obtains immediately $\lambda_1 = \lambda_2 = 0$ and $\lambda_3 = ||\,\Omega_0\,||^2$. In this case, so-called null-polarizations exist, as detailed for instance by Agrawal et al. (Agrawal, Boerner, 1989), producing vanishing power returns for the copolar or crosspolar radar channel.
  Random targets, on the other hand, have non-vanishing minimum eigenvalues λ_1 and λ_2 (rank(Σ) = 3) and, therefore, only minimisation rather than complete suppression of mean backscattered power can be achieved by appropriate choice of the transmitter polarization.
  Note the substantial differences for an area of grass (nearly deterministic) and an area of buildings (random) as shown in Figure 12 and Figure 13.

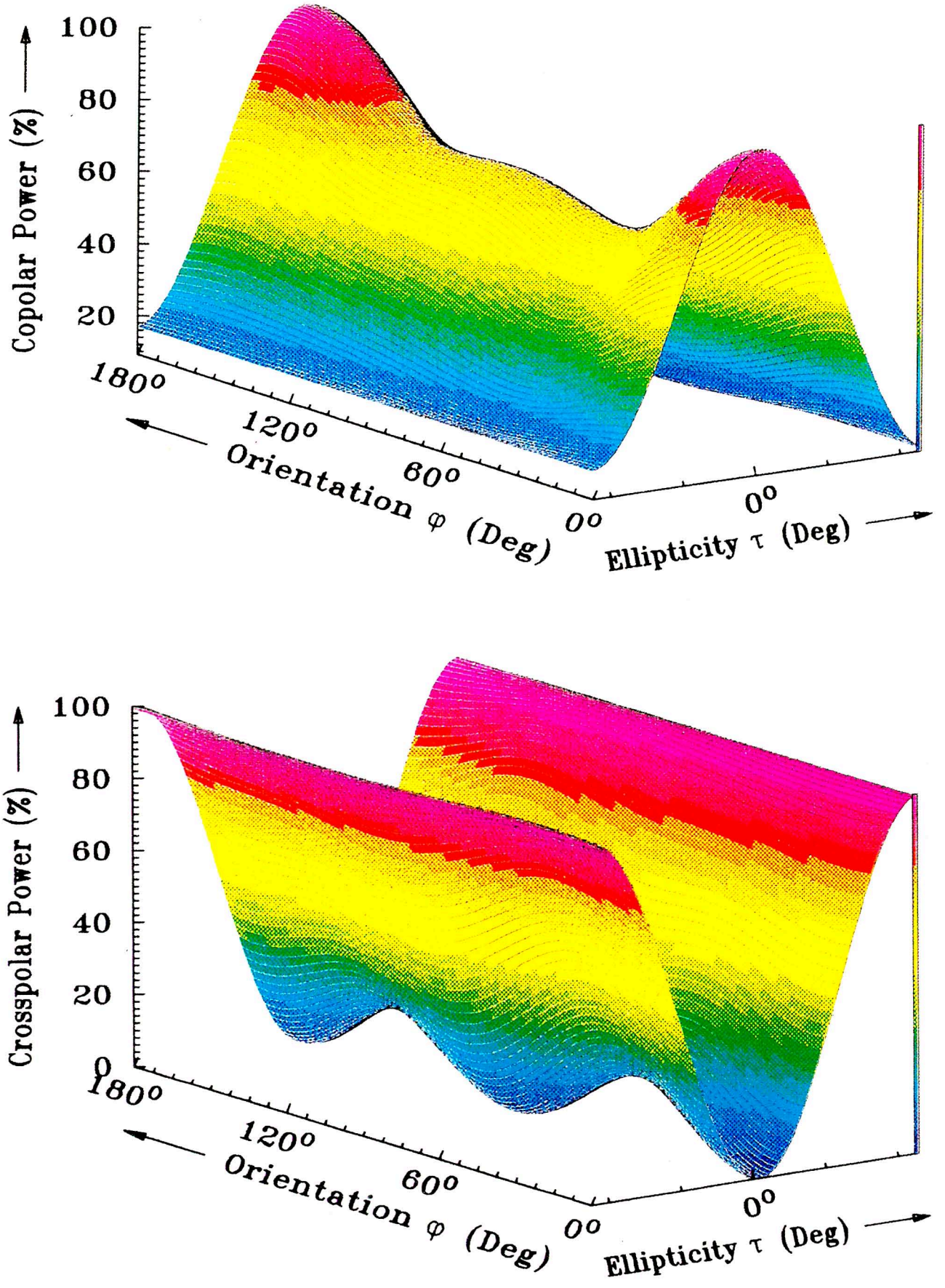

Fig. 12 - Copolar and Crosspolar Power Signatures for Grass Area.

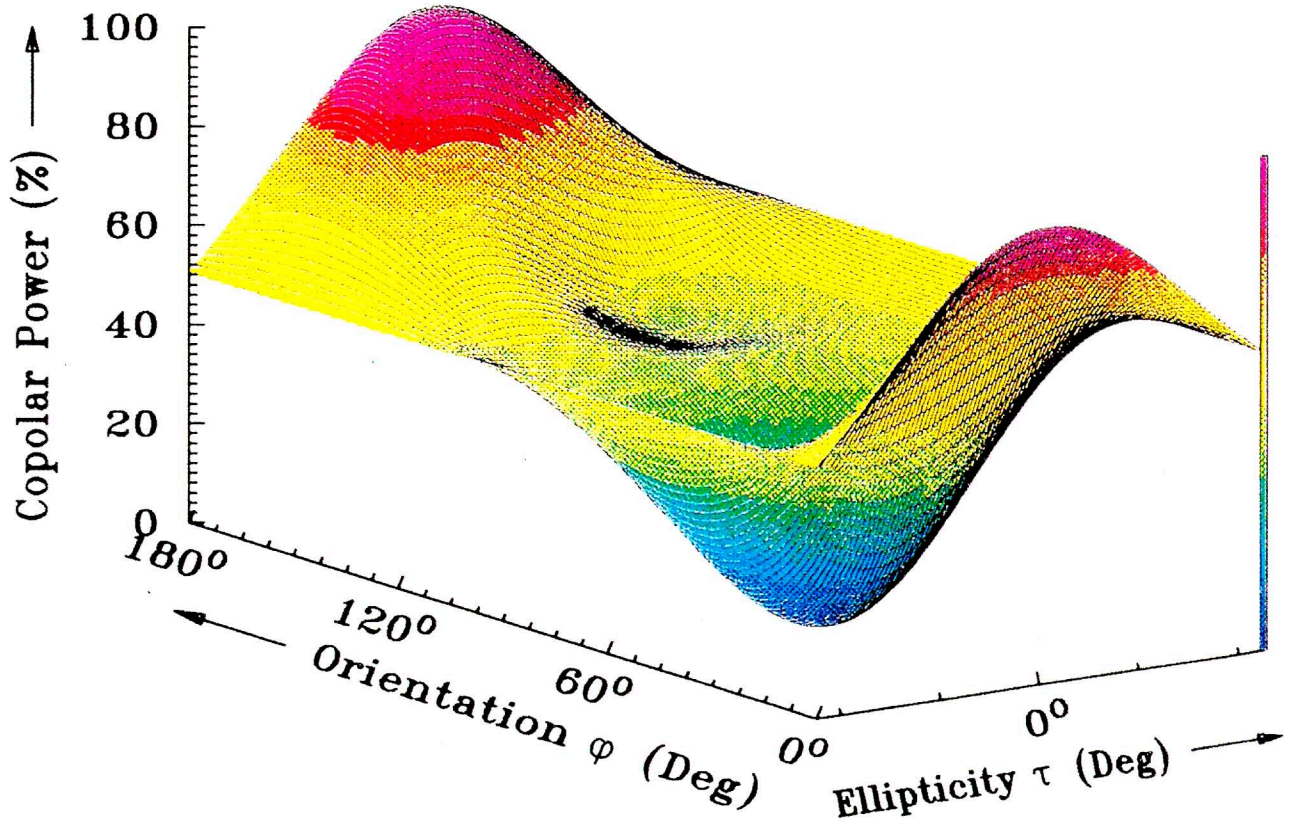

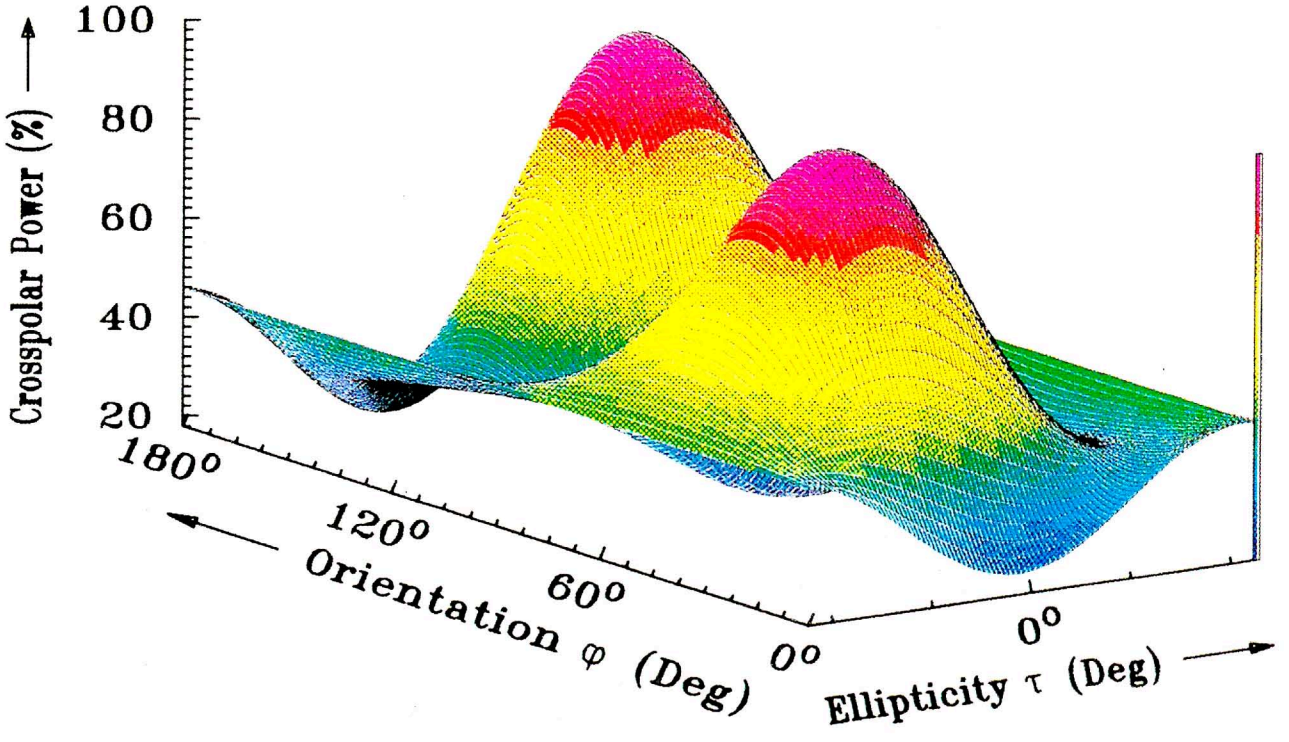

Fig. 13 - Copolar and Crosspolar Power Signatures for Area of Buildings.

- The eigenvalue difference

$$\Delta\lambda = \lambda_{max} - \lambda_{min} = \lambda_3 - \lambda_1 \quad (25)$$

of extremal eigenvalues λ_3 , λ_1 of the covariance matrix determines the range in which the mean power return $P_{co}^{A}(\rho)$ and $2P_x(\rho)$ can be varied by polarimetric means. It can be shown for a Hermitian matrix like the covariance matrix Σ that its field of values is

$$F(\Sigma) = F(\Sigma_0) = [\,\lambda_1\,,\,\lambda_3\,] \quad (26)$$

where $[\,\lambda_1\,,\,\lambda_3\,]$ denotes the segment from λ_1 to λ_3 on the real axis.

The field of values of a general matrix $A \in \mathbb{C}^{nxn}$ is defined as the set $F(A)$ of complex numbers (Lancaster, Tismenetsky, 1985)

$$F(A) = \{(Ax\,,\,x)\,|\,x^{+}x = 1\} \quad . \quad (27)$$

Setting $x = e_1 = [\,1,0,0\,]^T$ and similarly $x = e_2$ and $x = e_3$ the following bounds become immediately evident from eq. (22):

$$0 \le \lambda_1 \le P_{co}^{A}(\rho)\,,\,2P_x(\rho)\,,\,P_{co}^{B}(\rho) \le \lambda_3 \le ||\,\Omega_0\,||^2 \quad (28)$$

In general, minimal and maximal eigenvalues λ_1 , λ_3 of Σ cannot be realized by $P_{co}^{A}(\rho)$, $2P_x(\rho)$, $P_{co}^{B}(\rho)$, however, since the transformation matrix $T(\rho)$ of eq. (15) represents a restricted subset of all 3×3 unitary unimodular matrices.

Similar to the considered eigenvalue difference an indicator called coefficient of variation (ratio of minimum to maximum received power) has been introduced by van Zyl (van Zyl, 1986).

- From (14) follows that

$$\begin{aligned} &trace\,\Sigma = trace\,\Sigma_0 = trace < \Omega\,\Omega^{+} > = < trace\,\Omega\,\Omega^{+} > \\ &= < ||\,\Omega\,||^2 > = < span\,S > \\ &= < |\,S_{HH}\,|^2 > + 2 < |\,S_{HV}\,|^2 > + < |\,S_{vv}\,|^2 > \\ &= \lambda_1(\Sigma) + \lambda_2(\Sigma) + \lambda_3(\Sigma) \end{aligned} \quad (29)$$

is a polarization invariant quantity giving the total backscattered power in the four polarization configurations of a particular orthogonal basis.

CONCLUSION

This paper demonstrates the versatility and performance of polarimetric methods in the fields of radar remote sensing and microwave propagation.

It is shown how polarimetric radar measurements lead to better estimates of rain rate and microwave attenuation, and target classification descriptors obtained from covariance matrix analysis. The polarimetric effects in radiometric measurements of rain are provided in the form of differential sky noise temperature.

In the future, even more emphasis will be given to the problem of the calibration of polarimetric devices. Currently, a Polrimetric Active Radar Calibrator is in development at DLR. Enhanced calibration concepts, taking into special consideration the polarization purity of the transmitted signal, antenna pattern dependences, transfer characteristics of the transmitt-receive hardware and overall instrument stability, will allow the operational implementation of refined polarimetric tools and methods.

REFERENCES

Schroth A., Chandra M., and Meischner P., 1989, "A C-Band Coherent Polarimetric Radar for Propagation and Cloud Physics Research", J. Atmos, Ocean. Tech., Vol. 6(1), pp. 803-822.

Chandra M., Jank T., Meischner P., Schroth A., Clemens E., and Ritenberg F., 1986, "The Advanced Coherent Polarimetric DFVLR Radar", 23-rd Rad. Met. Conf., Am. Met. Soc., Snowmass, USA, pp. JP385-JP393.

Hendry A., and Mc Cormick G.C., 1974, "Polarization Properties of Precipitation Particles Related to Storm Structure", J. de Rech. Atmos, pp. 189-200.

Chandra M., Schroth A., and Lueneburg E., 1987, "Analysis and application of Weather-Radar S-matrix and M-matrix Measurements", ICAP-87, York, U.K., IEE Publ. No 274, pp. 328-333.

Chandra, 1991, "Prediction of Propagation Effects and Rain-Intensity using Radar Determined Three-Parameter Raindrop-Size Distribution", ICAP-91, York, U.K., IEE Publ. No. 333, pp. 88-94.

Chandra M., Schroth A., and Lueneburg E., 1985, "Three Parameter characterization of Raindrop-size Distributions by Coherent Polarimetric Radars", ICAP-85, Warwick, U.K., IEE Publ. No. 248, pp. 11-17.

Mitra S.K., Vohl O., and Pruppacher H.R., 1988, "A Wind Tunnel Study on the Melting of Snow Flakes", 10-th International Cloud Physics Conference, Bad Homburg, Germany; Conf. Preprints, Vol. 1, pp. 18-21.

Schnablel G., 1988, "Tropospheric Influences and Their Determination by Means of Radar Measurements", ESA-TT-1143, translation of DFVLR-FB 88-53.

COST project 205, "Influence of the Atmosphere on Radiopropagation on Satellite Earth Paths at Frequencies above 10 GHz", Physical Sciences, Comission of the European Communities, report EUR 9923 En.

Dissanayake A.W. and McEwan N.J., 1978, "Radar and Attenuation Properties of Rain and Bright Band", Proc. of ICAP '78, London.

CCIR (Study Group V), 1986, "Propagation Data and Prediction Methods Required for Earth-Space Telecommunication Systems", Recommendations and Reports, report no. 564-3.

Brussard G., 1984, "Radiometry, a Useful Prediction Tool?", ESA SP-1071.

Asayesh A., 1984, "Attenuation due to Rain at Millimeter and Centimeter Wavelenghts", University of Texas, Austin, USA.

Morrisson J.A., and Cross M.-J., 1974, "Scattering of a Plane Electromagnetic Wave by Axissymmetric Rain Drops", Bell Sys. Tech. J., 53, No. 6, 955-1019.

Atlas D., and Ullbrich C.W., 1977, "Path and Area Integrated Rainfall Measurements by Microwave Attenuation in the 1-3 cm Band", Journal of Applied Meteorology, Vol. 16, pp. 1322-1331.

Hornbostel A., Schroth A., Preissner J., 1991, "The DLR Station for Propagation Measurements on Earth Satellite Paths and First Results", Proc. ICAP '91, part 1, conference publ. no. 333, pp. 468-471.

Chandrasekhar S., 1960, "Radiative Transfer", Dover Publications, New York, USA.

Ishimaru A., and Cheung R.L.T., 1980, "Multiple-Scattering Effect on Radiometric Determination of Rain at Milimeter Wavelenghts", Radio Science, Vol. 15, No. 3, 507-516.

Born M., and Wolf E., 1964, "Principles of Optics", Pergamon Press, Oxford, U.K.

van Zyl J.J., 1986, "On the Importance of Polarization in Radar Scattering Problems", Ph.D. Dissertation, California Institute of Technology, Pasadena, USA.

Tragl K., 1990, "Polarimetric Radar Backscattering from Reciprocal Random Targets", IEEE Trans. Geosci. Remote Sensing, GE-28 (5), pp. 856-864.

Agrawal A.P., and Boerner W.-M., 1989, "Redevelopment of Kennaugh's Target Characteristic Polarization State Theory Using the Polarization Transformation Ratio Formalism for the Coherent Case", IEEE Trans. Geosci. Remote Sensing, GE-27 (1), pp. 2-14.

Held D.N., Brown W.E., Freeman A., Klein J.D., Zebker H., Sato T., Miller T., Nguyen Q., and Lou Y., 1988, "The NASA/JPL Multifrequency, Multipolarization Airborne SAR System", Proceedings of IGARSS '88 Symposium, vol. I, pp. 345-350., ESA SP-284, (IEEE 88CH2497-6).

Lancaster P., and Tismenetsky M., 1985, "The Theory of Matrices", 2. Edt., Academic Press, Orlando, USA.